THE ASTROPHYSICAL JOURNAL, 554:L173–L176, 2001 June 20

DISCOVERY OF X-RAY EMISSION FROM THE CRAB PULSAR AT PULSE MINIMUM

ALLYN F. TENNANT,[1] WERNER BECKER,[2] MICHAEL JUDA,[3] RONALD F. ELSNER,[1] JEFFERY J. KOLODZIEJCZAK,[1]
STEPHEN S. MURRAY,[3] STEPHEN L. O'DELL,[1] FRITS PAERELS,[4] DOUGLAS A. SWARTZ,[5]
NORIAKI SHIBAZAKI,[6] AND MARTIN C. WEISSKOPF[1]
Received 2001 March 22; accepted 2001 May 17; published 2001 June 19

ABSTRACT

The *Chandra X-Ray Observatory* observed the Crab pulsar using the Low-Energy Transmission Grating with the High-Resolution Camera. Time-resolved zeroth-order images reveal that the pulsar emits X-rays at *all* pulse phases. Analysis of the flux at minimum—most likely nonthermal in origin—places an upper limit ($T_\infty < 2.1$ MK) on the surface temperature of the underlying neutron star. In addition, analysis of the pulse profile establishes that the error in the *Chandra*-determined absolute time is quite small, -0.2 ± 0.1 ms.

Subject headings: ISM: individual (Crab Nebula) — pulsars: individual (Crab Pulsar) — radiation mechanisms: nonthermal — stars: neutron — X-rays: general

1. INTRODUCTION

The Crab pulsar ($P = 33.5$ ms) is the best studied, young ($t \approx 10^3$ yr) rotation-powered pulsar. To determine, inter alia, its pulse profile and to search for thermal emission from the underlying neutron star, we obtained phase-resolved observations of the Crab pulsar using the *Chandra X-Ray Observatory* (Weisskopf et al. 2000b). Due to the high surface brightness of the nebula, *Chandra*'s unprecedented angular resolution (<1″) is essential for achieving the required sensitivity.

First (§ 2), we describe the observations and data analysis, explaining the special processing necessary to extract the pulse profile for this very bright and rapidly varying source. We next (§ 3) address *Chandra*'s absolute timing accuracy and then (§ 4) scrutinize the pulse profile, discovering significant X-ray flux even at pulse minimum. Finally (§ 5), we discuss the results, concluding that the X-ray emission is predominantly nonthermal even at pulse minimum but setting an upper limit ($T_\infty < 2.1$ MK) to blackbody emission from the neutron star's surface.

2. OBSERVATIONS AND ANALYSIS

We obtained two observations of the Crab Nebula and pulsar, utilizing the *Chandra* Low-Energy Transmission Grating Spectrometer (LETGS)—the LETG with the High-Resolution Camera Spectroscopy (HRC-S) detector. Designated by Observation Identifiers (ObsIDs) 758 and 759, the observations acquired 100 and 50 ks of data on 2000 January 31 and February 2, respectively. For the longer observation, we employed an HRC-S spatial window only slightly larger than the nebula, to minimize telemetry saturation resulting from the nebula's brilliance and the high background. For the shorter observation, we used a larger spatial window spanning all three HRC-S segments, to obtain the dispersed spectrum. Table 1 gives the trigger rates, the "dead-time factor" (i.e., the live-time fraction), and the time-interval filter efficiency (described below).

Peculiarities in the raw pulse profile, found during initial analysis of these data, helped us to detect an HRC wiring error that results in assigning each trigger the time tag of the preceding trigger. If telemetry included data from all triggers, we could simply shift time tags to compensate. Unfortunately, it does not. At the high trigger rates for this source, the first-in-first-out (FIFO) buffer fills, thus dropping events until the readout frees slots in the buffer.

To mitigate this timing problem, we shift all time tags back one (reported) event and then apply a time-interval filter, thus bounding the arrival-time uncertainty. If no intervening triggers are lost, a back-one shift would yield precise timing. If intervening triggers are lost, the time tag will be that of the last lost trigger, which must have occurred *after* the correct time of the event in question. Hence, the shifted time tag must be either correct or late, but never early. Obviously, the time of the event must also be later than the time assigned to the previous (reported) event. Thus, if two (reported) events differ in (assigned shifted) time by δt, then the time of the second event must be accurate to better than δt. Consequently, we apply a time-interval filter of duration Δt to bound this uncertainty. The time-interval filter necessarily reduces the efficiency, thus requiring a correction (Table 1) for the fraction of events passed by the filter.

To verify our understanding of the instrument and treatment (including time-interval filtering) of the data, we constructed a Monte Carlo simulator. This high-fidelity simulator accounts for various delays and dead times inherent in the HRC, including the FIFO and its interaction with the telemetry readout. Input to the simulator comprises four data streams. Two unpulsed components represent nebular X-rays and non–X-ray background, which require separate treatment because of differing onboard rejection rates. Two pulsed components represent zeroth-order and dispersed/scattered pulsar X-rays, the latter affecting dead time although not contributing to the zeroth-order image. For the pulse template, we use an appropriately adjusted (see Fig. 1 legend) pulse profile from *ROSAT* High-Resolution Imager (HRI) observations.

Figure 1 illustrates our analysis and use of the simulator to confirm the analysis. The figure shows the pulse-profile data with the spline fitted for *ROSAT*-HRI data (*top*), for simulated *Chandra*-HRC data through a 2 ms time-interval filter (*middle*),

[1] Space Science Department, NASA Marshall Space Flight Center, NASA/MSFC/SD50, Huntsville, AL 35812.
[2] Max-Planck-Institut für extraterrestrische Physik, Giessenbachstrasse, Postfach 1312, D-85740 Garching, Germany.
[3] Smithsonian Astrophysical Observatory, 60 Garden Street, Cambridge, MA 02138.
[4] Columbia Astrophysics Laboratory, Columbia University, 538 West 120th Street, New York, NY 10027.
[5] Universities Space Research Association, NASA Marshall Space Flight Center, USRA/MSFC/SD50, Huntsville, AL 35812.
[6] Rikkyo University, 3-34, Nishi-Ikebukuro, Tokyo 171-8501, Japan.

TABLE 1
HRC-S Count Rates

ObsID	Trigger Rate (s^{-1})	Dead-Time Factor	Time-Filter Efficiency
758	638	0.739	0.282
759	636	0.364	0.152

and for ObsID 758 *Chandra*-HRC data, within 1.″32 of the pulsar, through a 2 ms filter (*bottom*). The filtered *Chandra* data (simulated and actual) differ very little from the (adjusted) *ROSAT* pulse-profile template. Indeed, the only significant residuals (in the trailing portions of the main pulse) occur in both simulated and actual *Chandra* 2 ms–filtered data. An analysis of the second *Chandra* data set (ObsID 759) produces similar results.

3. ABSOLUTE TIMING

Before discussing the pulsar flux detected at all pulse phases, we address *Chandra*'s timing accuracy. W. S. Davis (2000, private communication) used on-orbit measurements to verify that *Chandra*'s ultrastable oscillator easily meets the relative-accuracy requirement of 10^{-9} over 24 hr and achieves this stability over much longer periods by carefully correlating the spacecraft clock with UTC as recorded by a ground station. Relativistic corrections are insignificant; calculating the light-travel time delay is straightforward. That different ground sites—each with its own internal delay—give consistent results indicates that ground delays are also correct.

Checking delays internal to the spacecraft is more difficult. The spacecraft records the clock value at the start of generating a telemetry packet. This packet remains in a buffer until complete, whereupon it enters the telemetry stream. Because packets cover about a quarter second of data, their latency is about 0.25 s, depending on the telemetry rate. W. S. Davis has shown that these delays—preflight verified by calculation only—yield inconsistent results, varying by 0.16 ms as the telemetry rate changes from 32 to 1024 kbit s^{-1}. Current processing uses the calculated delay for 512 kbit s^{-1} and applies corrections for other telemetry rates to make the clock correlation consistent. There is no assurance that the absolute value of the correction is correct. Our measurements here and our comparison with results from other X-ray satellites (below) are the first attempt to establish the *Chandra* absolute timing accuracy.

We reference times to the solar system barycenter using two independent codes: (1) the *Chandra* X-ray Center program axBary (using the -ref FK5 option to match the radio position) and (2) a code based on the Starlink software SLALIB (Wallace 1994) and a JPL routine that interpolates the JPL DE200 planetary ephemeris. These two codes give results agreeing to within 0.025 ms. For the accuracy required here, we ignore this slight difference as well as an additional 0.020 ms delay in the HRC circuitry.

The Jodrell Bank Observatory routinely observes (Lyne, Pritchard, & Smith 1993) the Crab pulsar (primarily at 610 MHz) and publishes its period ephemeris.[7] Upon applying a 2 ms filter to the *Chandra* data and folding according to the radio ephemeris, the X-ray flux peaks at phase 0.984 (with a formal error <0.001) for each *Chandra* data set. Thus, the X-ray pulse leads the radio by about 0.54 ms (0.016 of its 33.5 ms period), consistent with phase values (0.980–0.998) found in a careful analysis (Rots, Jahoda, & Lyne 2000) of *Rossi X-Ray Timing Explorer* (*RXTE*) data. A. Rots (2001, private communication) has analyzed the *RXTE* data obtained the day before our *Chandra* observation and finds a phase of 0.991 ± 0.002. We eliminated ambiguities modulo the pulse period by cross-correlating simultaneous *RXTE* and *Chandra* observations of the rapid burster. Hence, the *Chandra*-determined phase of the Crab pulsar relative to the *RXTE*-determined phase bounds the error in the *Chandra* absolute time to $(t_{Chandra} - t_0) = -0.2 \pm 0.1$ ms.

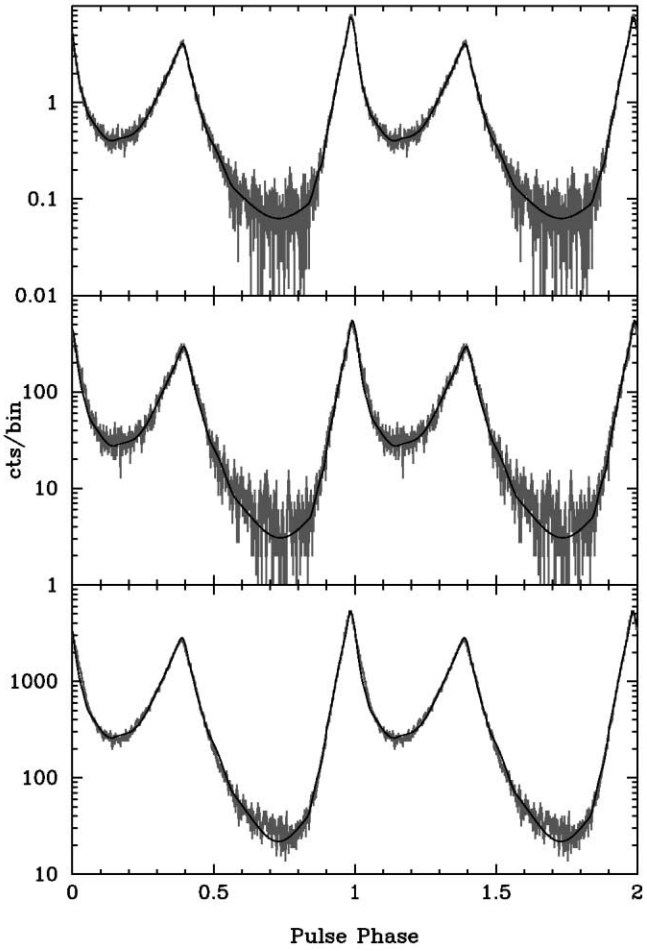

Fig. 1.—X-ray pulse profiles of the Crab pulsar, in 250 phase bins, referenced to radio phase zero. The top panel displays the *ROSAT* HRI observation, with the spline fitted to the data. The middle panel shows the *Chandra* simulation for a 2 ms filter, compared to a *ROSAT*-derived template with adjusted phase, DC offset, and normalization. The bottom panel gives actual *Chandra* data from ObsID 758, after application of a 2 ms filter, compared with a *ROSAT*-derived template with adjusted phase, DC offset, and normalization.

4. PULSE PROFILE

The *Chandra*-measured, 2 ms–filtered profile (Fig. 1, *bottom*) shows significant flux at pulse minimum. This discovery is even more manifest in the image itself. Figure 2 shows the 2 ms–filtered, LETGS zeroth-order image at pulse maximum and at pulse minimum. We note that the centroid positions of the point source in the two images are identical to within 0.1 HRC pixel—0.013, or 0.15 lt-day at 2 kpc.

To determine the Crab pulsar's minimum flux from the raw count rate, we must correct for the nebular "background," the point-spread function, and dead-time and time-interval filter efficiencies. Due to *Chandra*'s superb angular resolution, we

[7] Available at http://www.jb.man.ac.uk/~pulsar/crab.html.

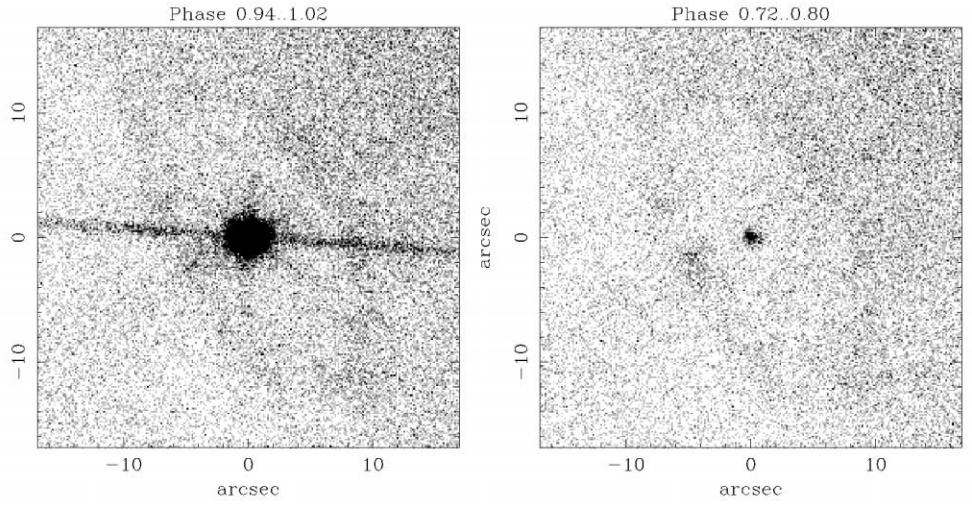

FIG. 2.—*Chandra* images of the Crab pulsar (ObsID 758) at pulse maximum and minimum. The line visible at pulse maximum (phases 0.94–1.02, *left*) is the spectrum dispersed by LETG fine-support bars. The pulsar is clearly visible, even at pulse minimum (phases 0.72–0.80, *right*); the inner ring of the nebula is also apparent.

can use a small (1″.32 radius) aperture to reduce the nebular contribution while capturing most pulsar X-rays. Indeed, the nebular background—determined within an ellipse delineated by the inner ring (Fig. 2)—contributes only 17% of the counts within the aperture; the point source—with 95% of its flux within the aperture—contributes the remaining 83%. Although corrections for dead time and 2 ms filtering are substantial (Table 1), the demonstrated fidelity of the simulator (Fig. 1) gives us confidence in their accuracy. At pulse minimum, then, the *corrected* LETGS zeroth-order count rate is 0.19 ± 0.01 (± 0.02) counts s^{-1}. The quoted errors denote formal statistical (estimated systematic) uncertainties.

In measuring the minimum pulsar flux, we begin at phase 0.72, which is more than 2 ms (0.06 phase) after the phase historically considered as the beginning of the off-pulse. Thus, our results can be contaminated only by flux that was previously unobservable. We also determined the (corrected) count rate for filter durations of 0.5, 1.0, 2.0, and 4.0 ms. As the duration decreased from 2 to 0.5 ms, the filtered count rate decreased by 10%. Thus, our quoted count rate is based on the minimum, and 10% is our estimate of the systematic uncertainty.

The main goal of our *Chandra* observations was to improve upon the *ROSAT* limit on the pulsar flux at minimum (Becker & Aschenbach 1995). Surprisingly, the count rate for the *Chandra* detection exceeds that corresponding to the *ROSAT* upper limit. Two factors contributed to the erroneous *ROSAT* bound. First, the inner nebular ring (Fig. 2 and Weisskopf et al. 2000a) and *ROSAT*'s poorer angular resolution conspired to smooth the apparent nebular surface brightness in the *ROSAT* images, greatly reducing the contrast between the pulsar and the adjacent nebula. Second, an error in the *ROSAT* analysis led to substantial underestimation of the statistical uncertainty. Taking into account these two factors, the *ROSAT* data are consistent with the *Chandra* detection. In particular, the *Chandra* image at pulse minimum yields a flux agreeing with the total *ROSAT* count rate in the *ROSAT* aperture.

Finally, before interpreting the data, we remark that a simple empirical model, comprising superposed exponential waveforms, fits the pulse profile over all phases (Fig. 1) very well. The primary pulse has equal 0.9 ms rise and decay time constants; the secondary pulse has 2.2 ms rise and 1.2 ms decay time constants. Furthermore, the fluences (integrated flux) in the primary and secondary pulses are quite comparable. After removing these two pulses, the remaining flux is consistent with a single 12 ms exponential decay (starting at pulse phase zero), both in the "bridge" (phases 0.08–0.24) and in the "interpulse" (phases 0.72–0.80).

5. DISCUSSION

We believe that the X-ray flux at pulse minimum is predominantly nonthermal, as at other pulse phases. First, the X-ray profile is similar to the visible-light one, which is also detected in all pulse phases (Golden, Shearer, & Beskin 2000a; Golden et al. 2000b; Peterson et al. 1978) and cannot be thermal. Indeed, although the Crab pulsar's pulse profile does exhibit weak energy dependence, the basic pattern persists over 7 orders of magnitude in photon energy (e.g., Eikenberry et al. 1997; Massaro, Feroci, & Matt 1997). Second, the pulse profile (consistent with superposed exponential waveforms) indicates no temporally constant component—i.e., it does not "bottom out" as it would if a constant component dominated the flux at minimum. Third, analysis of LETGS first-order spectra (in preparation) suggests that the pulsar's X-ray emission is nonthermal, even at minimum flux. At pulse minimum, the dispersed spectrum contains only about 100 pulsar photons—mostly between 1 and 2 keV—against a nebular background of about 500. Nonetheless, the spectral data are adequate to show that any soft thermal component contributes few of the detected photons.

The (corrected) measured count rate (0.19 counts s^{-1}) does, however, bound any thermal emission. To estimate this upper limit, we consider blackbody emission from the surface of a neutron star. We express the spectral flux in terms of "observable" parameters—namely, the temperature T_∞ and angular size θ_∞ determined by a distant observer. Doing so, the unattenuated blackbody spectral flux depends only on T_∞ and θ_∞:

$$F_E(E; T_\infty, \theta_\infty) = B_E(E; T_\infty)\pi\theta_\infty^2, \quad (1)$$

where $B_E(E; T)$ is the blackbody spectral intensity. We use the *Chandra* PIMMS tool to propagate this spectral flux through an interstellar column $N_{\rm H}$ and the effective area $A_{\rm eff}(E)$ cor-

responding to the LETG–HRC-S zeroth-order response function. Comparison of the resulting model count rate with the (corrected) observed count rate $\dot{c}$ then constrains T_∞ for given θ_∞ and $N_{\rm H}$.

As a representative case, take $\theta_\infty = 2.1 \times 10^{-16}$ rad—for $R_\infty = 13$ km (e.g., $R_s = 10$ km and $M = 1.4\ M_\odot$) at $D = 2$ kpc—and $N_{\rm H} = 3 \times 10^{21}$ cm^{-2}. With these parameters, the blackbody temperature that would account for all the flux at minimum is $T_\infty = 2.12$ MK $= 0.183$ keV, which bounds the actual temperature. A linearized sensitivity analysis establishes that the computed temperature $T_\infty \propto \dot{c}^{+0.19}\theta_\infty^{-0.38}N_{\rm H}^{+0.21}$ near this value, so it is rather insensitive to the count rate and to specific parameters used. More difficult to quantify are consequences of departures from uniform, isotropic, blackbody emission (see Pavlov et al. 1994, 2000; Zavlin et al. 1995; Becker & Pavlov 2001). Hence, we regard $T_\infty \approx 2.1$ MK and the associated luminosity—$L_\infty \approx 2.4 \times 10^{34}$ ergs s^{-1}—as indicative upper limits to the thermal component.

The *Chandra-detected* flux at pulse minimum then bounds $T_\infty < 2.1$ MK for the Crab pulsar's underlying neutron star. Hence, existing X-ray observations of this young ($t \approx 10^3$ yr) neutron star can exclude only a few of the competing models for neutron star cooling (Becker & Pavlov 2001; Tsuruta 1998 and references therein; Potekhin, Chabrier, & Yakovlev 1997; Chabrier, Potekhin, & Yakovlev 1997; Schaab et al. 1997, 1999; Schaab, Weber, & Weigel 1998b; Schaab & Weigel 1998; Schaab, Balberg, & Schaffner-Bielich 1998a; Yakovlev, Kaminker, & Levenfish 1999; Baiko & Haensel 2000).

Detailed analyses of existing and proposed LETGS first-order spectra (in preparation) will help us better define the X-ray spectrum of the Crab pulsar at all pulse phases. These analyses will allow a modest reduction of the upper limit on the temperature of an isothermal, blackbody neutron star and of more realistic models for neutron star thermal spectra. The relatively high interstellar column strongly attenuates the low-energy ($E < 0.5$ keV) X-rays, so that detectable thermal X-rays are well into the Wien portion of the blackbody distribution for relevant temperatures. Hence, the count rate for a blackbody component deceases exponentially with $(E/T) > 1$, so that the upper limit to T_∞ depends very weakly on the accumulated counts. The analysis presented here relies solely on LETGS zeroth-order data, which contain *no* spectral information. Consequently, these data cannot exclude higher temperature thermal emission from a small fraction of the neutron star's surface—such as from hot polar caps (e.g., Pavlov et al. 2000; Chakrabarty et al. 2001).

Finally, we remark on the impressively good description of the *Chandra*-determined pulse profile that the simple superposition of exponential waveforms provides (§ 4). Accounting for this pulse profile and relating it to the profile in other energy bands (e.g., Eikenberry et al. 1997; Massaro et al. 1997; Golden et al. 2000a, 2000b) could constrain models for IR–γ radiation from pulsars.

We thank Bill Davis (Computer Sciences Corporation, at the *Chandra* Operations Control Center) for furnishing detailed information on spacecraft clock stability and timing delays. We also thank Mark Roberts and Michael Kramer (Jodrell Bank Observatory) for supplying a Crab pulsar radio ephemeris matched to our observing periods and Arnold Rots (*Chandra* X-ray Center) for providing the *RXTE*-determined X-ray phase for 2000 January 30.

REFERENCES

Baiko, D. A., & Haensel, P. 2000, A&A, 356, 171
Becker, W., & Aschenbach, B. 1995, in The Lives of the Neutron Stars, ed. M. A. Alpar, Ü. Kiziloğlu, & J. van Paradijs (Dordrecht: Kluwer), 47
Becker, W., & Pavlov, G. 2001, in The Century of Space Science, ed. J. Bleeker, J. Giess, & M. Huber (Dordrecht: Kluwer), in press
Chabrier, G., Potekhin, A. Y., & Yakovlev, D. G. 1997, ApJ, 477, L99
Chakrabarty, D., Pivovaroff, M. J., Hernquist, L. E., Heyl, J. S., & Narayan, R. 2001, ApJ, 548, 800
Eikenberry, S. S., Fazio, G. G., Ransom, S. M., Middleditch, J., Kristian, J., & Pennypacker, C. R. 1997, ApJ, 477, 465
Golden, A., Shearer, A., & Beskin, G. M. 2000a, ApJ, 535, 373
Golden, A., Shearer, A., Redfern, R. M., Beskin, G. M., Neizvestny, S. I., Neustroev, V. V., Plokhotnichenko, V. L., & Cullum, M. 2000b, A&A, 363, 617
Lyne, A. G., Pritchard, R. S., & Smith, F. G. 1993, MNRAS, 265, 1003
Massaro, E., Feroci, M., & Matt, G. 1997, A&AS, 124, 123
Pavlov, G. G., Shibanov, Y. A., Ventura, J., & Zavlin, V. E. 1994, A&A, 289, 837
Pavlov, G. G., Zavlin, V. E., Aschenbach, B., Trümper, J., & Sanwal, D. 2000, ApJ, 531, L53
Peterson, B. A., Murdin, P., Wallace, P., Manchester, R. N., Penny, A. J., Jorden, A., Hartley, K. F., & King, D. 1978, Nature, 276, 475
Potekhin, A. Y., Chabrier, G., & Yakovlev, D. G. 1997, A&A, 323, 415
Rots, A. H., Jahoda, K., & Lyne, A. G. 2000, AAS HEAD Meeting, 32, 33.08
Schaab, C., Balberg, S., & Schaffner-Bielich, J. 1998a, ApJ, 504, L99
Schaab, C., Hermann, B., Weber, F., & Weigel, M. K. 1997, ApJ, 480, L111
Schaab, C., Sedrakian, A., Weber, F., & Weigel, M. K. 1999, A&A, 346, 465
Schaab, C., Weber, F., & Weigel, M. K. 1998b, A&A, 335, 596
Schaab, C., & Weigel, M. K. 1998, A&A, 336, L13
Tsuruta, S. 1998, Phys. Rep., 292, 1
Wallace, P. T. 1994, in ASP Conf. Ser. 61, Astronomical Data Analysis Software and Systems III, ed. D. R. Crabtree, R. J. Hanisch, & J. Barnes (San Francisco: ASP), 481
Weisskopf, M. C., et al. 2000a, ApJ, 536, L81
Weisskopf, M. C., Tananbaum, H. D., Van Speybroeck, L. P., & O'Dell, S. L. 2000b, Proc. SPIE, 4012, 2
Yakovlev, D. G., Kaminker, A. D., & Levenfish, K. P. 1999, A&A, 343, 650
Zavlin, V. E., Pavlov, G. G., Shibanov, Y. A., & Ventura, J. 1995, A&A, 297, 441